Title
MATHEMATICAL MODELING OF LITHIUM(ALLOY), IRON DISULFIDE CELLS

Authors
Bernardi, D.
Newman, J.

Publication Date
1986-06-01

Lawrence Berkeley Laboratory

UNIVERSITY OF CALIFORNIA

Materials & Molecular Research Division

Submitted to Journal of the
Electrochemical Society

MATHEMATICAL MODELING OF LITHIUM(ALLOY),
IRON DISULFIDE CELLS

D. Bernardi and J. Newman

June 1986

Prepared for the U.S. Department of Energy under Contract DE-AC03-76SF00098

DISCLAIMER

LBL-21764

Mathematical Modeling of Lithium(alloy), Iron Disulfide Cells

Dawn Bernardi* and John Newman

Materials and Molecular Research Division,
Lawrence Berkeley Laboratory, and
Department of Chemical Engineering,
University of California,
Berkeley, California 94720

June 24, 1986

Abstract

Results obtained from computer programs simulating the behavior of $LiAl/FeS_2$ and $Li(Si)/FeS_2$ high temperature molten salt cells are presented. The models predict the cell voltage, temperature, and heat-generation rate during cell operation. Position-dependent behavior, such as reaction rates and concentrations within the cell, is also calculated. The models predict operational characteristics and determine the influence of changes in design parameters on the performance of the cells. The effects of state of discharge, initial electrolyte composition, temperature, and discharge current density on cell behavior are investigated. Factors that can limit a cell during operation are identified. The cell discharge behavior is compared with available experimental data. The models clarify our understanding of these battery systems and can help guide experimental research.

Key words: Cell model, high-temperature battery, molten salt

* Present address: General Motors Research Laboratories, Warren, Michigan 48090-9055

Introduction

Secondary, high-temperature batteries employing molten-salt electrolytes based on lithium as the negative electrode and sulfur as the positive electrode were conceived for electric vehicle propulsion and energy storage applications. The melting point of the electrolyte in these cells usually restricts the operating temperatures to above 400°C. The stationary energy storage applications include off-peak storage for electric utility systems (also referred to as load leveling) and the storage of energy produced by wind or sun.[1] The incentive for the development of these systems is the extremely high open-circuit potential and theoretical energy density of the Li/S couple (2.23 V and 2602 W-hr/kg, respectively).[2] The Li/S cell, which was invented in 1968 at Argonne National Laboratory,[1] posed several engineering difficulties associated with the high lithium and sulfur activities. The advantages of using a molten-salt electrolyte over an aqueous electrolyte include reducing electrolyte decomposition, ohmic resistance, and mass-transfer limitations. High-temperature operation also promotes faster electrode reactions relative to cells operated at lower temperatures. The disadvantages to operating at high temperatures are increased corrosion of cell components and increased volatility and solubility of active material. In Li/S cells, these same disadvantages are aggravated by the high lithium and sulfur activities, and the liquid lithium electrode is difficult to contain. In 1973, these problems were lessened by substituting solid, $\alpha-\beta$ LiAl alloy for the lithium in the negative electrode and FeS for the sulfur in the positive electrode, at the expense of a lower cell voltage and energy density.[2] Later, the Li(Si)/FeS_2 couple was proposed as a higher voltage and higher power alternative to the LiAl/FeS cell. It should be noted, however, that the theoretical specific energy of a Li(Si)/FeS_2 cell operating only on the uppermost FeS_2 voltage plateau (and the relevant plateaus of the Li(Si) electrode) is 434.5 W-hr/kg, while the theoretical specific energy of a LiAl/FeS system (with the negative electrode operating over a composition range which allows a fair comparison) is 436.4 W-hr/kg. The higher potential of the Li(alloy)/FeS_2 cell, however, reduces the number

of cells per battery and increases the maximum power achievable relative to the LiAl/FeS cell. Also, the Li(Si) electrode has more usable lithium content than the LiAl electrode. (Li(alloy) will refer to either LiAl or Li(Si).) The Li(Si)/FeS_2 cells share some of the disadvantages of the Li/S system associated with the increased activities of lithium and sulfur relative to LiAl/FeS cells.

Currently, lithium(alloy), iron sulfide batteries require further development in order to reach commercial acceptability. We believe that theoretical efforts combined with experimental investigations provide an efficient method of development. Modeling these cells can aid in design and development by identifying system limitations and investigating the influence of changing operating parameters on cell performance. Mathematical models also contribute to a more fundamental understanding of battery systems. The comparison of model to experimental results helps substantiate our understanding of the systems.

A mathematical model of the LiAl/LiCl-KCl/FeS cell was developed by Pollard and Newman[3,4,5] in 1979. Much of their work was done in conjunction with experimental investigations at Argonne National Laboratory. We have developed a mathematical model of the Li(alloy)/FeS_2 cell from Pollard and Newman's model. The galvanostatic discharge behavior of the cell constitutes the main emphasis of this work. The thermodynamic behavior of the lithium(alloy)/FeS_2 cell is also discussed in this treatment.

Thermodynamic Behavior of Li(Si)/FeS_2 Cells

The description of the thermodynamic behavior of Li(alloy)/FeS_2 cells can aid in the understanding, development, and design of these cells. An investigation of the thermodynamic, open-circuit potential behavior of the Li(Si)/FeS_2 cell as a function of state-of-discharge, temperature, and negative-to-positive capacity ratio is presented in this section. This thermodynamic information is derived from open-circuit electrode potentials which are available in the literature. The thermodynamic data on the FeS_2 electrode and the Li(Si) electrode are combined

in the examination of the open-circuit potential behavior for reversible-isothermal discharge of a Li(Si)/FeS_2 cell.

The intermediate phases of the FeS_2 electrode are the subject of some controversy. Tomczuk *et al.*[6] at Argonne National Laboratory have accomplished some of the most recent work with this electrode. In their work, the authors summarize the controversy, and we feel that they also resolve a great deal of it. We make use of their work in the construction of the Li(alloy)/FeS_2 cell model. The researchers combined metallography and x-ray diffraction methods. Photomicrographs of coexisting electrode phases were examined, and the complex reaction sequences were identified. Recently, another controversy has evolved regarding the FeS_2 electrode. The work of Schmidt and Weppner[7,8] contradicts Argonne's work. This controversy has not been discussed in the literature.

The compositions of the intermediate phases in the Li-Si system have also been subject to some controversy. We believe that the work of Wen and Huggins[9] resolves this disagreement. These researchers use the equilibrium coulometric titration technique in the determination of the composition dependence of the Li(Si) electrode potential and X-ray diffraction analyses to characterize the intermediate phases.

The Li-Fe-S Phase Diagram.—Figure 1 gives the phase diagram for the Li-Fe-S system that is in accordance with Argonne's[6] data. Table 1 shows the reactions for the four regions of discharge of an FeS_2 electrode. (Electrochemical reactions are written for the three-phase regions of discharge, and the two-phase region will be discussed later.) In contrast to the FeS electrode,[10,11] the overall cell reactions do not involve the electrolyte phase. Consequently, the regions are conveniently shown on a ternary phase diagram, and the open-circuit potentials relative to a Li, a LiAl, or a Li(Si) reference electrode are independent of the amount and composition of the electrolyte. The numbers on the phase diagram refer to the number of solid phases of

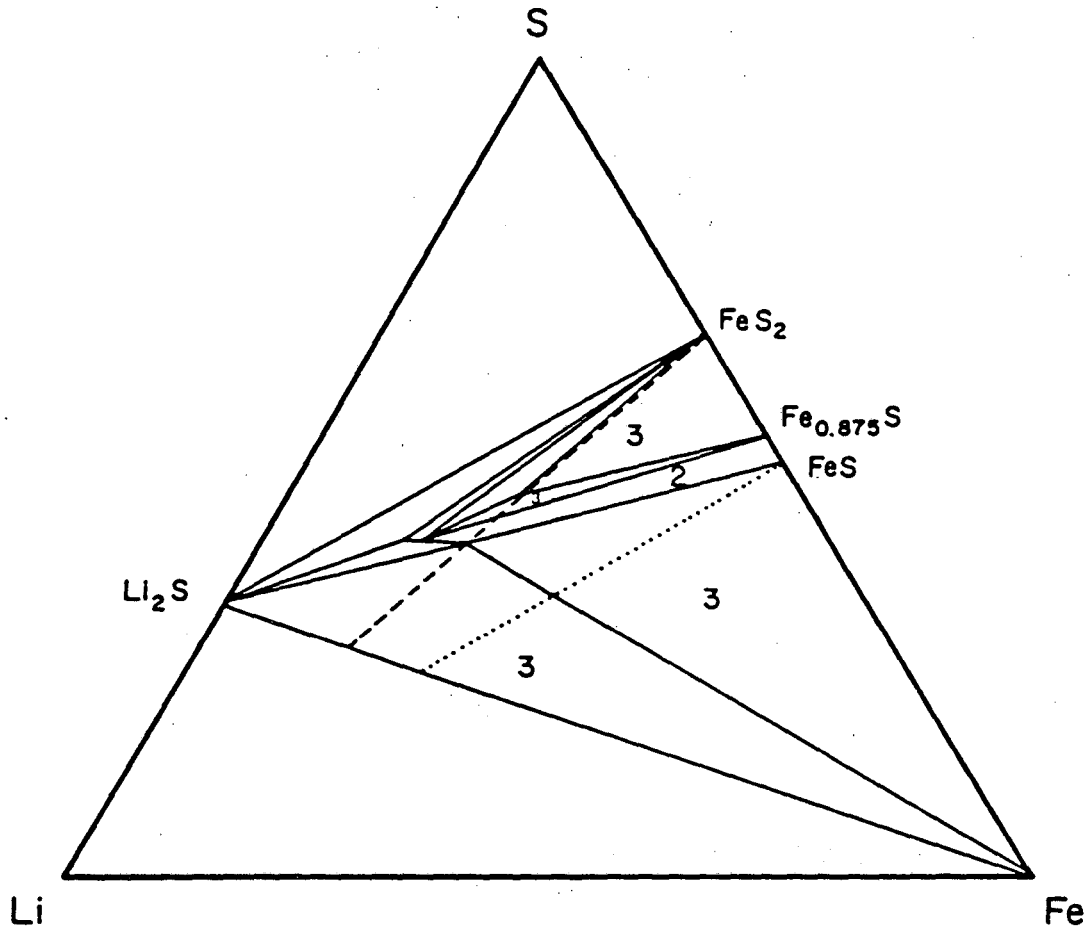

Figure 1. Ternary phase diagram for the Li-Fe-S system as given by Tomczuk *et al.*[6] The numbers are in regions of particular interest and indicate the number of phases in equilibrium.

Table 1. Electrochemical Reactions of the FeS_2 Electrode at 450°C [6]

Region	
a.	$2FeS_2 + 3Li^+ + 3e^- \rightarrow Li_3Fe_2S_4$
b.	$Li_3Fe_2S_4 + 0.47Li^+ + 0.47e^- \rightarrow 1.58Li_{2.2}Fe_{0.8}S_2 + 0.84Fe_{0.875}S$
c.	$Fe_{1-x'}S$ and $Li_{2+x}Fe_{1-x}S_2$ produce Li_2FeS_2
d.	$Li_2FeS_2 + 2Li^+ + 2e^- \rightarrow 2Li_2S + Fe$

the positive electrode in equilibrium when the overall composition of the system is within the region. The addition of lithium to an Fe-S system corresponds to moving along a line connecting the Fe-S composition to the pure-lithium corner of the triangle. Therefore, the reversible discharge of an FeS_2 electrode corresponds to moving along the dashed line in Figure 1. The dashed line passes through four regions. The regions correspond to regions a through d in Table 1. It is helpful to think of the dashed line as beginning just below pure FeS_2. That is, beginning with a minor amount of the $Fe_{0.875}S$ phase. The reason for this will be discussed later. Region a is within the FeS_2-$Li_3Fe_2S_4$-$Fe_{0.875}S$ triangle. Region b is the thin triangle representing the $Li_3Fe_2S_4$-$Fe_{0.875}S$–$Li_{2.2}Fe_{0.8}S_2$ equilibrium. Region c is a two-phase region. At the beginning of this region, $Fe_{0.875}S$ and $Li_{2.2}Fe_{0.8}S_2$ are in equilibrium. Within the two phase region, the phases $Fe_{1-x'}S$ and $Li_{2+x}Fe_{1-x}S_2$ are in equilibrium. At the end of region c, virtually all the $Fe_{1-x'}S$ has disappeared, and only Li_2FeS_2 remains. In passing through the two-phase region, the composition variables x and x′ range from 0.2 to 0 and 0.125 to 0, respectively. The final region of discharge, region d, is the Li_2FeS_2-Li_2S-Fe three-phase triangle. Li_2S and Fe are the final products of the complete discharge of an FeS_2 electrode. The potentials of the FeS_2 electrode in

regions a and d are frequently called the upper-upper and lower voltage plateau, respectively. The voltage behavior in regions a, b, and c are sometimes lumped together and referred to as the upper voltage plateau.

We can compare the FeS_2 electrode discharge sequence with the discharge of an FeS electrode. The dotted line in Figure 1 represents the discharge of the FeS electrode (ignoring J-phase). There are two regions of discharge shown for this electrode. The first region is the FeS-Li_2FeS_2-Fe phase triangle. The second region is the same as region d of FeS_2 discharge. Discharge of the FeS electrode through this final region occurs with a larger iron content than the discharge of the FeS_2 electrode through the same region. In actuality, this simple, two-reaction sequence would occur at a much higher temperature ($>$ 641.5°C)[10,12,13]; at 450°C the intermediate phase $LiK_6Fe_{24}S_{26}Cl$ (J-phase) is also a stable discharge product of the FeS electrode.

We will not include any potassium-containing compounds in our treatment of the FeS_2 electrode. Experimental measurements indicate, however, that for the equilibrium discharge of an FeS_2 electrode in eutectic electrolyte, minor amounts of J-phase are formed in region d.[6] Tomczuk *et al.* postulate that the slow chemical conversion of the electrochemically produced Li_2FeS_2 (X-phase) to J-phase accounts for this. The evolution of sulfur vapor during discharge (which allows FeS to form) can also lead to the formation of J-phase via the reaction of FeS with the electrolyte. Tomczuk *et al.* also indicate the presence of small amounts of the potassium containing compound $KFeS_2$ in the nonequilibrium discharge of the FeS_2 electrode.

The Gibbs phase rule can be applied to the FeS_2 electrode (at a constant temperature and pressure) to show that there is only one degree of freedom for region c, and zero degrees of freedom for regions a, b, and d. In other words, reactions a, b, and d in Table 1 are characterized by potential plateaus, and region c has an open-circuit potential that varies with utilization of the electrode material. In this two-phase region, the solid phases change composition as the elec-

trode is discharged.

We describe the temperature dependence of the open-circuit potential in the three-phase regions with an equation of the form

$$U_l = a_l + b_l T \ . \tag{1}$$

Table 2 gives the literature data for the coefficients in this equation corresponding to reactions a, b, and d in Table 1. With these coefficients, and temperature in kelvins, Equation 1 will give the potential in volts. All the electrode reaction potentials are given relative to a two-phase ($\alpha-\beta$) LiAl-alloy reference electrode. The data in this table are for eutectic composition of electrolyte; however, the open-circuit potentials of all the reactions relative to the ($\alpha-\beta$) LiAl reference electrode should be independent of electrolyte composition.

The reaction sequences described above are for the temperature of 450°C. The temperature dependency of the Fe-S system is well characterized.[16] The length of the single-phase portion of

Table 2. Coefficients for the Open-Circuit Potential of the FeS_2 Electrode

Region	a_l [V]	$b_l \times 10^3$ [V/K]
a.	1.4251[14]	0.4785[14]
b.	1.208771[15]	0.65142[15]
d.	1.43211[11]	-0.147[11]
3.	1.3389[11]	0.133[11]

the Fe-S leg ($Fe_{1-x}S$ phase) will increase as the temperature is increased (up to 1015 K). The solid-solution phase $Li_{2+x}Fe_{1-x}S_2$ is not observed at room temperature. It is believed that this compound decomposes on cooling into $Li_{2.33}Fe_{0.67}S_2$ and Li_2FeS_2.[6]

The solid line in Figure 2 is a plot of the thermodynamic open-circuit potential of the $LiAl/FeS_2$ cell as a function of positive electrode utilization at 450°C. The dotted line is for a LiAl/FeS cell (ignoring J-phase). This plot was constructed with the information given in Tables 1 and 2, and with the assumption of a linear potential variation through the two-phase region c. The open-circuit potential at each end of this region is well characterized. The potential at the upper end of the region is given by the data for region b in Table 2. The potential at the lower end is given by the data for reaction three. As shown in Figure 2, this is also the potential of the first plateau for discharge of the FeS electrode. The data for the two end points of region c can be combined to give

$$U_c = U_b + \frac{(a_3 - a_b) + T\,(b_3 - b_b)}{1 - [2.2(4x'_o - 2\,)/(2x'_o - 0.8) - 3]} \left(\frac{q_c\, 2\, \widetilde{V}_{FeS_2}}{\epsilon^o_{FeS_2} F} \right), \tag{2}$$

for the open-circuit potential behavior as a function of temperature and state-of-discharge q_c (the number of coulombs of charge passed for reaction c per unit volume of the electrode, see Equation 7). As we discussed earlier, the value of x'_o (0.875 at 450°C) is a function of temperature. The data for the Fe-S system[16] can be used, and we can estimate x'_o to have the following linear temperature dependence:

$$x'_o = -9.240 \times 10^{-5}\, T + 0.91658\,. \tag{3}$$

The numbers 2.2 and 0.8 in Equation 2 arise from the formula of the compound $Li_{2.2}Fe_{0.8}S_2$ phase, which is assumed to be independent of temperature.

In Figure 2, region a of discharge terminates at 37.5% utilization, and region b terminates at approximately 42% utilization. The sloping potential region, region c, terminates at 50%

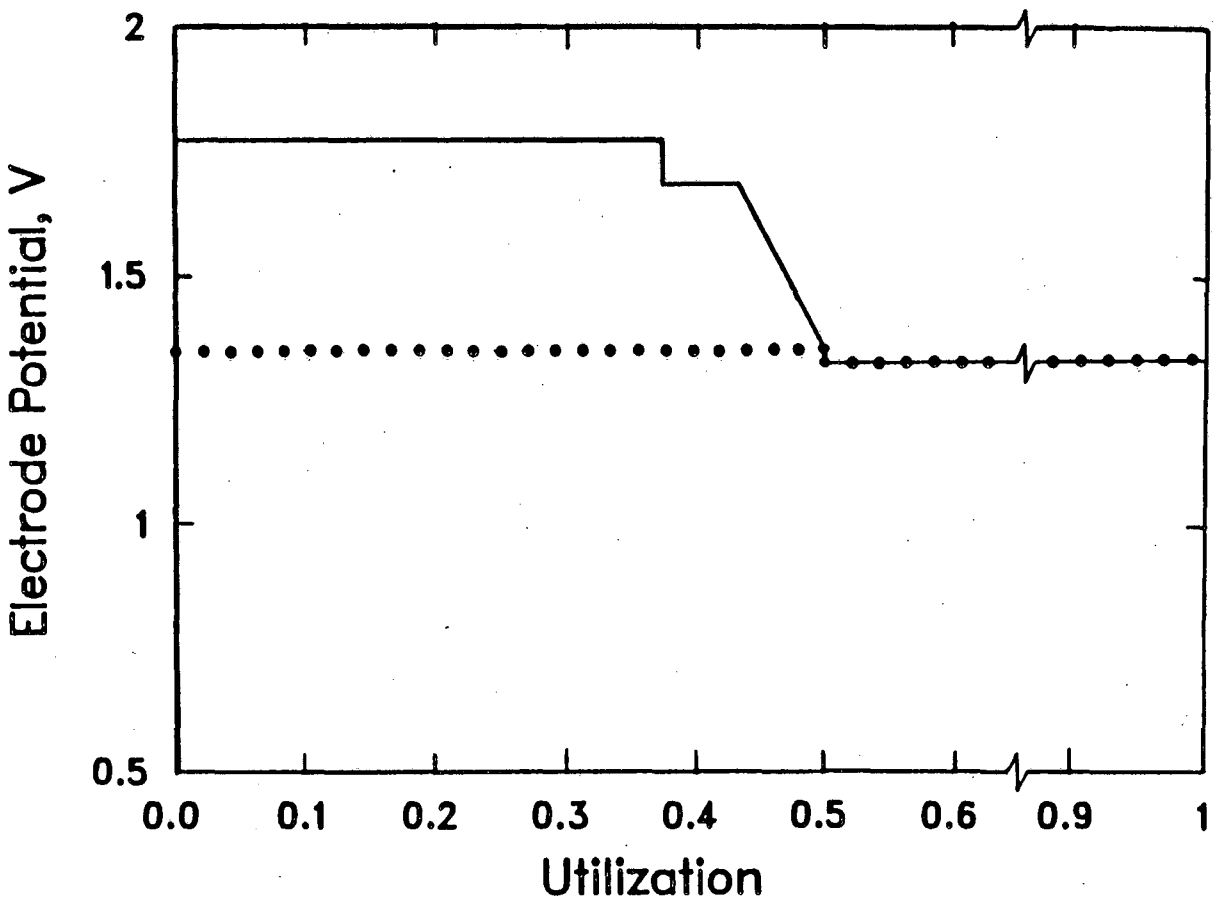

Figure 2. Thermodynamic, open-circuit potential as a function of positive electrode utilization at 450°C. The solid line is for a LiAl/FeS_2 cell. The dotted line is for a LiAl/FeS cell.

utilization of FeS_2. One may actually consider the FeS_2 electrode to have yet another region of discharge with a small capacity within the FeS-Li_2FeS_2-Fe triangle, which is responsible for the vertical drop in potential at the end of region c. As shown in Figure 2, this potential drop is equivalent to the gap in plateau voltages for the LiAl/FeS cell. It arises because the dashed line in Figure 1 touches the corner of the Li_2FeS_2–FeS–Fe three-phase triangle. The width of the region would increase with increases in the ratio of $Fe_{0.875}S$ to FeS_2 at the beginning of discharge. In this work we shall assume that there is always an infinitesimally small amount of the $Fe_{0.875}S$ at the beginning of discharge to avoid discharge along the boundary in region a.

In experimental cells, a constant FeS_2 electrode potential is obtained with discharge along the FeS_2–$Li_3Fe_2S_4$ boundary of the FeS_2–$Li_3Fe_2S_4$–$Fe_{0.875}S$ triangle (Figure 1). These experimental cells utilize stoichiometric FeS_2 as the starting material. However, the potential during discharge along the boundary would be unstable. There are at least two explanations for this observed constant potential. The first possibility is the loss of sulfur due to the evolution of sulfur vapor. The dashed line in Figure 1 does not describe the discharge of an FeS_2 electrode with sulfur evolution. The discharge line would be shifted downward (away from the S corner) and perhaps develop curvature depending on the sulfur content at each point during the discharge. $Fe_{0.875}S$ would then be a product of the first reaction, and capacity in the FeS–Li_2FeS_2–Fe region would appear during discharge. Since FeS can react electrochemically to form J-phase, this may explain the presence of J-phase in experimental cells.

A second possible explanation is that the boundary may actually be a narrow, two-phase region. For example, the compound $Li_3Fe_2S_4$ may have some range of iron and sulfur composition. Thus, $Li_3Fe_2S_4$ would be represented by a corner of a two-phase triangle within the phase diagram. The discharge along this two-phase, FeS_2-$Li_3Fe_2S_4$ boundary would give a stable, constant potential. On the diagram then, another two-phase triangle would also exist between the boundary of the first two-phase region and the $Li_{2.2}Fe_{0.8}S_2$ phase.

For the sake of simplicity, the solubility of lithium in $Fe_{1-x}S$ is omitted from Figure 1. During discharge through region c in experimental cells, minor amounts of lithium are detected in the $Fe_{1-x}S$ phase.[15] That is, the single-phase portion of the Fe-S side of the triangle in Figure 1 has some width in lithium composition. Consequently, the FeS_2—$Fe_{0.875}S$ two-phase field would also have some width.

The Li_2S—FeS_2—S region of Figure 1 was not investigated by Tomczuk *et al.* The potential in this region can be calculated from the Gibbs free energies of the components.[17] The calculations give 1.88 V versus the LiAl reference electrode. This value agrees with the experimental data of Schmidt and Weppner.[7]

The phase diagram of the Li-Fe-S system is derived from the work of Tomczuk *et al.* from Argonne National Laboratory. We use their work in our calculations. One major conclusion in Schmidt and Weppner's work contradicts the work of Tomczuk *et al.*: Schmidt and Weppner claim that Li_2FeS_2 is the only ternary compound in the Li-Fe-S phase diagram; they do not agree with the existence of the $Li_3Fe_2S_4$ phase. They consider the reaction of FeS_2 to Li_2FeS_2 to occur in region a. They claim that X-phase has a wide range of nonstoichiometry, indicated by a sloping potential region in their coulometric titration data.[7,12] They show a 10% variation in lithium content about Li_2FeS_2. The stoichiometry given by Tomczuk *et al.* shows a 20% variation in lithium content from $Li_3Fe_2S_4$ to Li_2FeS_2 (through region c). To summarize, the two studies agree that an FeS_2 electrode would encounter a sloping potential region on discharge. However, the position and width of the region are not in agreement. It should be noted that Tomczuk *et al.* did their experimentation at a temperature 50°C higher than Schmidt and Weppner. It is possible that the range and position of the sloping potential region are functions of temperature. Experimental cells distinctly show a second voltage plateau at 37% utilization, which supports the existence of the $Li_3Fe_2S_4$ phase. More research is required to resolve the discrepancies in the two pieces of work. In Reference 12, a more complete comparison of References 6 and 7 is

given.

The Phase Behavior of Li(Si) at 450°C.—Figure 3 gives a plot of the potential of a Li(Si) electrode relative to a two-phase LiAl reference electrode as given by a Wen and Huggins.[9] Table 3 gives the corresponding electrochemical reactions and coefficients for the form of the open-circuit potential given in Equation 1. The potential is given in volts, and the temperature is in kelvins. Sharma and Seefurth[18] give the temperature dependence of the potential plateaus. The reactions are written according to the phase compositions given by Wen and Huggins.

The equilibrium discharge of a Li(Si) electrode is shown by moving to the left in Figure 3 from a chosen starting material. We have designated three regions of discharge. Each region is a two-phase region and is characterized by a potential plateau (at constant temperature and pressure). For example, starting with the $Li_{3.25}Si$ alloy, the removal of lithium on discharge will form the $Li_{2.33}Si$ phase. When the starting material is exhausted, potential plateau II is reached.

Table 3. Reactions and Coefficients for the Open-Circuit Potential of the Li(Si) Electrode

Reaction		a_l* [V]	$b_l \times 10^3$* [V/K]
I	$Li_{3.25}Si \rightarrow Li_{2.33}Si + 0.92Li^+ + 0.92e^-$	-0.187529	0.0731
II	$Li_{2.33}Si \rightarrow Li_{1.71}Si + 0.62Li^+ + 0.62e^-$	-0.088097	0.1122
III	$Li_{1.71}Si \rightarrow Si + 1.71Li^+ + 1.71e^-$	-0.0345	0.1056

*a_l and b_l were obtained from Reference 18.

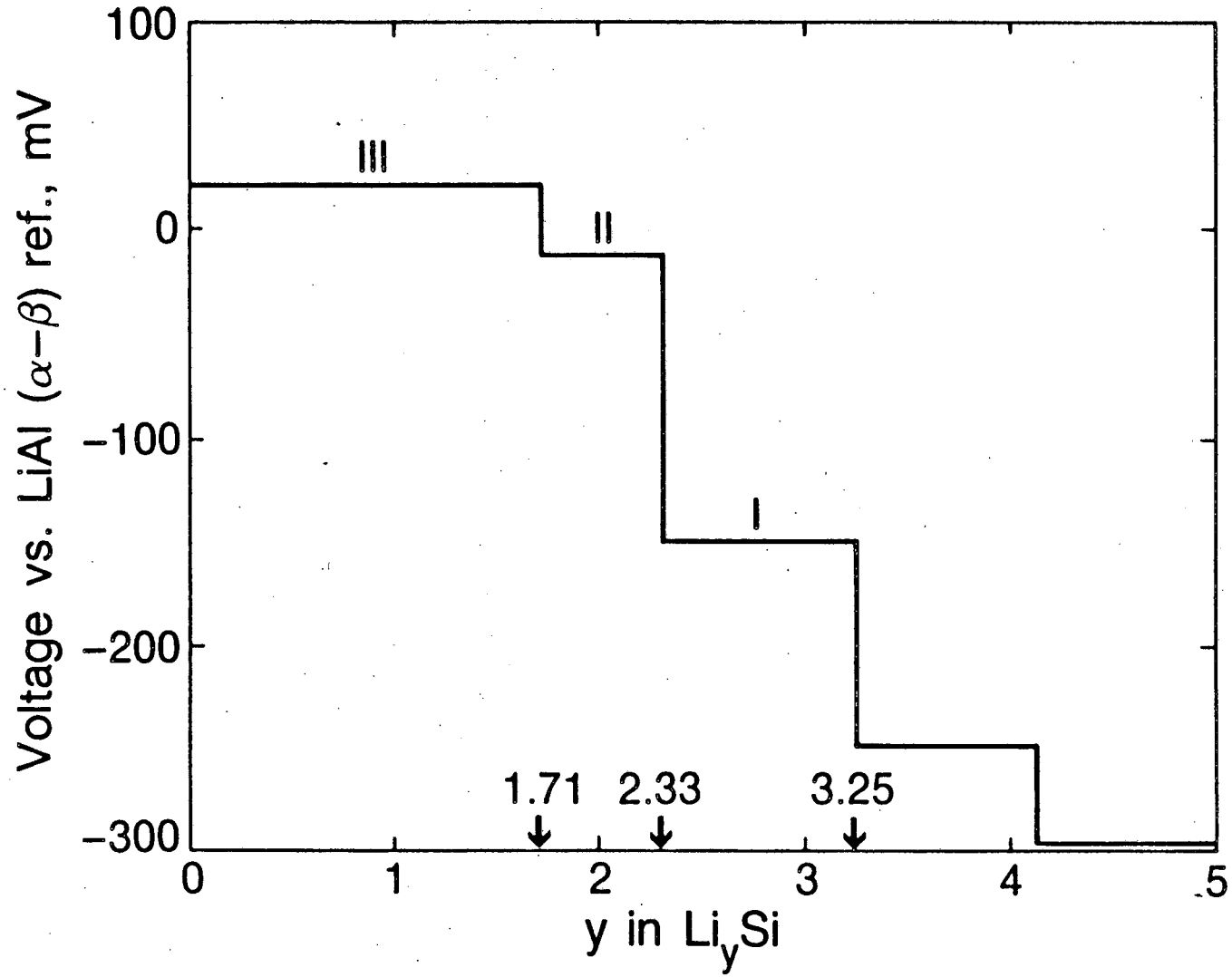

XBL 861-9403

Figure 3. Coulometric titration curve providing potential as a function of Li(Si) electrode composition at 400°C.[9]

If more lithium is removed from the $Li_{2.33}Si$ phase, the $Li_{1.71}Si$ phase is formed. The exhaustion of the $Li_{2.33}Si$ allows the potential to rise to plateau III. In this region, the $Li_{1.71}Si$ is in equilibrium with essentially pure silicon.

There are several aspects that should be considered in the design of a Li(Si) electrode. The $Li_{4.4}Si$ alloy is not a desirable starting material because it is unstable and cannot be handled effectively in a dry room. Also, discharge through region III should be avoided because the electrode has a high specific resistance is this region.[19]

In Figure 3 the potential appears to rise vertically between plateaus. The vertical portions on this figure, however, are actually narrow single-phase regions. Wen and Huggins investigated these narrow regions of nonstoichiometry and gave values of the chemical diffusion coefficient of lithium in the each region. The width of the $Li_{3.25}Si$, $Li_{2.33}Si$, and $Li_{1.75}Si$ single-phase regions corresponds to $\Delta y = 0.028$, 0.06, and 0.008, respectively. In our work with the Li(Si) electrode, we ignore the width of the single-phase regions.

The Open-Circuit Potential Behavior of Li(Si)/FeS_2 Cells.—The data in Tables 1 and 2 and Equations 2 and 3 are used to calculate the open-circuit potential behavior of a Li(Si)/FeS_2 cell. All of the results are presented for a cell with the capacity limited by the FeS_2 electrode. Figure 4 illustrates the open-circuit potential behavior as a function of positive-electrode utilization. The cell is discharged reversibly and isothermally at 725 K (452°C) for different values of the parameter β, the mole ratio of $Li_{3.25}Si$ to FeS_2. For a large value of β, we expect to see the positive-electrode behavior reflected in the discharge of a Li(Si)/FeS_2 cell. This is the case in Figure 4 for $\beta = 8.7$. As the value of β is decreased, we would expect to see more of the negative-electrode behavior during discharge.

In Figure 4, for the case of $\beta = 8.7$, the first drop in potential at 37.5% utilization is caused by the positive electrode going from region a to region b. The sloping potential region

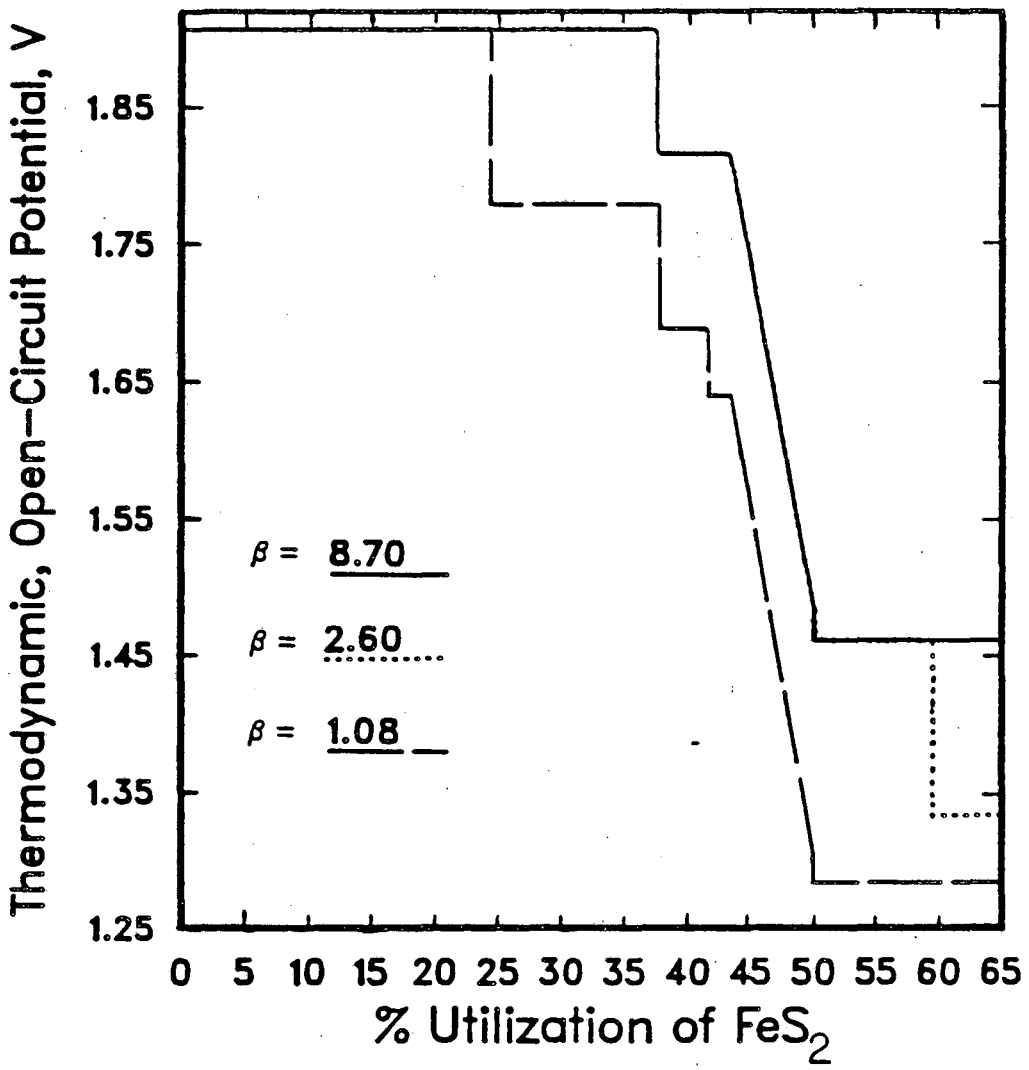

Figure 4. Calculated open-circuit potential behavior as a function of positive electrode utilization for a Li(Si)/FeS_2 cell at 725 K. In each curve, the ratio of negative to positive electrode starting material β is varied.

reflects the positive electrode going through region c (the two-phase region). At 50% utilization, the positive electrode reaches region d, the final plateau. Discharge with $\beta = 2.6$ is similar to the case with $\beta = 8.7$, except for the extra potential drop at 60% utilization. This potential drop reflects the behavior of the negative electrode going from region I to region II. For the case of $\beta = 1.08$, the corresponding potential drop occurs much earlier in the discharge (at 22% utilization). The second potential drop stems from the positive electrode going from region a to region b, the third potential drop marks the negative electrode entering region III, and the remainder of discharge reflects the behavior of the positive electrode. For the case with $\beta = 1.08$, the capacity of the negative electrode almost matches the capacity of the positive electrode. As we discussed earlier, discharge through region III of the Li(Si) electrode is undesirable because of the high resistance of the pure silicon phase. One may reject the design of this cell based on the results of Figure 4 alone.

If the temperature is increased for the case with $\beta = 1.08$, then the open-circuit potentials for the first four plateaus are increased. The open-circuit potential of the final plateau decreases with increasing temperature.

With these thermodynamic data, we can also examine the heat-generation rate for the reversible, isothermal discharge of a Li(Si)/FeS_2 cell.[12] This can give insight into the heating or cooling that may be required to maintain isothermal operation of a cell, which is an important aspect of cell design.

Model Development

The model of the Li(alloy)/LiCl,KCl/FeS_2 cell is developed from Pollard and Newman's model[3,4,5] for the LiAl/LiCl-KCl/FeS cell.

The galvanostatic discharge behavior of the Li(alloy)/FeS_2 cell constitutes the main emphasis of this work. We describe the mathematical model and the modifications that have been made to the original work of Pollard and Newman.[3,4] Model results for the Li(alloy)/FeS_2 cell are given, and comparisons with experimental results available in the literature are made.

A cross section of a cell sandwich is shown schematically in Figure 5. The model is one dimensional and consists of a porous negative electrode (shown on the left) and a porous positive electrode (shown on the right) with a reservoir and separator in between. The hatched area in the electrodes refers to the cell's active material (called the matrix phase). The clear area refers to molten LiCl-KCl electrolyte that fills the pores within the cell. The negative electrode can be either LiAl or Li(Si). The fundamental equations are material-balance equations for species in the electrolyte phase and electrode matrix phase, a modified Ohm's law equation, a current balance equation, and electrochemical-kinetic equations. The equations are cast into finite difference form, along with the appropriate boundary conditions, and solved iteratively by the method of Newman.[20] The Fortran computer code for the cell model is given in Reference 12.

FeS_2 Electrode Behavior.—If the FeS_2 electrode is discharged reversibly, then a single electrode reaction occurs within each region, corresponding to the reactions given in Table 1. The irreversible discharge of the electrode allows the reactions to occur simultaneously.

We shall first discuss the incorporation of the kinetic expressions for the reactions of the FeS_2 electrode. A polarization equation of the form

$$j_l = a i_{o,l} \left(e^{\alpha_{a,l} F \eta_{s,l}/RT} - e^{-\alpha_{c,l} F \eta_{s,l}/RT} \right) \tag{4}$$

is used, where

$$\eta_{s,l} = \eta - U_{l,o} \tag{5}$$

represents the local surface overpotential and η is defined as the electrode potential minus the

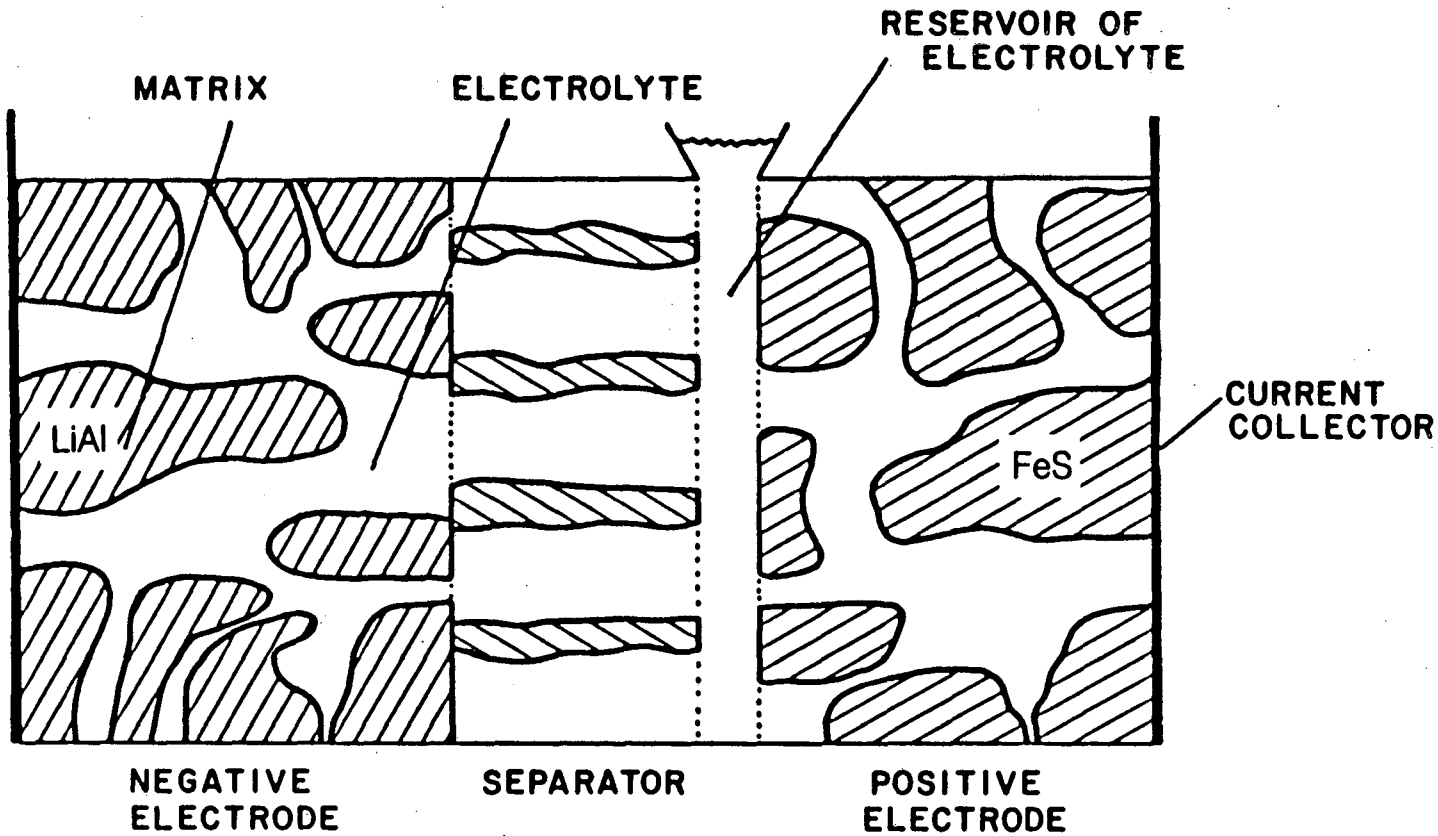

$$LiAl \rightarrow Li^{+} + e^{-} + Al$$

$$2FeS + 2Li^{+} + 2e^{-} \rightarrow Li_2 FeS_2 + Fe$$

Figure 5. Schematic diagram of the cell model. The electrochemical reactions shown correspond to discharge of the LiAl/FeS cell.

electrolyte potential. The quantity $U_{l,o}$ is the theoretical, open-circuit cell potential for reaction l, relative to a reference electrode of the same kind as reaction b, shown in Table 1, at the composition prevailing locally. It follows that $\eta_{s,l}$ is $\eta - (U_a - U_b)$, η , and $\eta - (U_d - U_b)$ for the reactions in regions a, b, and d, respectively. The values of U_l are given by Equation 1 along with the coefficients given in Table 2.

The kinetic equation for the reaction in region c is more complicated than the other reactions because the surface overpotential is dependent on the extent to which the reaction has occurred. The surface overpotential is given by

$$\eta_{s,c} = \eta - (U_c - U_b), \tag{6}$$

where U_c is defined by Equation 2 and

$$q_c = \int_o^t j_c \, dt \, . \tag{7}$$

The behavior of the intermediate phases in the discharge of an FeS_2 electrode is fairly complex. In the mathematical model, we simplify the phase transitions. In the material balance for the matrix phase, we assume that the phase transitions that occur as a result of the transfer currents j_b and j_c are approximated by the single transition

$$Li_3Fe_2S_4 + Li^+ + e^- \rightarrow 2\ Li_2FeS_2 \, . \tag{8}$$

The volume fraction of Li_2FeS_2 (X-phase) is calculated at each time step. One can think of this phase as being a lumped phase composed of the solid solution phases $Fe_{1-x'}S$ and $Li_{2+x}Fe_{1-x}S_2$. The molar volume of the lumped phase is assumed to be that of Li_2FeS_2 (X-phase). The approximation becomes accurate as reactions b and c approach completion. At this point, the amount of $Fe_{1-x'}S$ approaches zero and the $Li_{2+x}Fe_{1-x}S_2$ phase has the composition Li_2FeS_2 (x = 0). We do not have molar volume data for the $Li_{2+x}Fe_{1-x}S_2$ compound as function of the composition variable x.

We use the same argument for the calculation of the matrix conductivity; the conductivity of the lumped phase is assumed to be that of Li_2FeS_2. The matrix conductivity expression is developed in Reference 12.

Li(Si) Electrode Behavior.—As we discussed earlier, in the discharge of a $Li_{3.25}Si$ electrode, three regions can be distinguished. The mathematical model simulates the first region; the region in which the reaction

$$Li_{3.25}Si \rightarrow Li_{2.33}Si + 0.92\ Li^+ + 0.92\ e^-$$

occurs. The simulation of the Li(Si) electrode is, therefore, virtually identical to the treatment of the LiAl electrode. The $Li_{3.25}Si$ alloy is analogous to β-LiAl, and the $Li_{2.33}Si$ alloy is analogous to α-Al. Initially, it is assumed that the negative electrode matrix consists of nonporous, spherical particles of $Li_{3.25}Si$. On discharge, the outermost region of the particle reacts first, and a layer of $Li_{2.33}Si$ is formed which thickens gradually as the discharge proceeds. We refer the reader to the work of Pollard and Newman[3,4] for the mathematical description of this process.

A more complete description of the electrode behavior would include the reaction

$$Li_{2.33}Si \rightarrow Li_{1.71}Si + 0.62\ Li^+ + 0.62\ e^-, \tag{9}$$

which occurs in the second region. The reaction in the third region should also be incorporated; however, the high resistivity of the pure silicon phase makes this reaction undesirable. The Li(Si) electrode is twice as thick as the LiAl electrode in the mathematical model simulations, because plateau II wasn't treated in the model.

Operating Parameters.—We give some of the base-case operating conditions and data required for the FeS_2 model in Table 4. Many of the operating parameters are the same parameters that were used in Pollard and Newman's original work.[3,4] For example, the operating variables of the LiAl electrode are unchanged, and we refer the reader to Pollard and Newman's

work for all of these values (Figure 9 of Reference 4).

Deviations from the values in Table 4 will be noted in the figure captions. The kinetic parameters, $i_{o,l}$, $\alpha_{a,l}$, and $\alpha_{c,l}$, for the FeS and FeS_2 electrode reactions are the same. The thermodynamic data in Table 2 and Equation 2 are included in the model.

The molar volume data of some phases in the FeS_2 electrode are given in Table 5. The crystalographic data that are used to calculate the molar volumes are given in Reference 6.

We assumed the values of 4 and 12 for the formulas per unit cell (given in the fifth column of Table 5) of the $Li_{2.33}Fe_{0.67}S_2$ and $Fe_{0.875}S$ compounds, respectively. If we compare the molar volumes of these compounds to that of Li_2FeS_2 and FeS (18.55 and 46.23 cm^3/mole,[3,4] respectively), we see that our assumptions seem consistent. As we mentioned earlier, several simplify-

Table 4. Physical Parameters and Base-Case Input Data for the LiAl/FeS_2 Cell Model

Quantity	Value	Quantity	Value
σ_{Li_2S}	0 $(\Omega\text{-cm})^{-1}$	σ_{Fe}	8.23×10^4 $(\Omega\text{-cm})^{-1}$
σ_Z	0.2 $(\Omega\text{-cm})^{-1}$	σ_X	5.1 $(\Omega\text{-cm})^{-1}$
σ_{FeS_2}	100 $(\Omega\text{-cm})^{-1}$	i	0.0416 A/cm^2
L_+	0.21458 cm	T_o	743.15 K
$\epsilon^o_{FeS_2}$	0.245	$U_{a,o}$	0.0878 V
ϵ^o_+	0.755	$U_{b,o}$	0.0 V
$\epsilon_{ccp}\sigma_{ccp}$	2.1819 $(\Omega\text{-cm})^{-1}$	$U_{d,o}$	-0.37 V
m	1/3	U_b	1.6929 V

Table 5. Molar Volume Data for the Phases in the FeS_2 Electrode

Compound	M_i g/mol	crystal habit	unit cell volume $(\mathring{A})^3$	formulas per unit cell	$\widetilde{V}_i$ cm^3/mol
FeS_2	119.975	cubic	158.956	4	23.93
$Li_3Fe_2S_4$	260.767	monoclinic	164.65	1	99.17
Li_2FeS_2	133.853	hexagonal	82.72	1	49.82
$Li_{2.33}Fe_{0.67}S_2$	117.713	hexagonal	249.55	4	37.58
$Fe_{0.875}S$	80.930	hexagonal	368.44	12	18.49
Li_2S	45.942	fcc	186.37	4	28.062

ing assumptions have been made concerning the solid-phase material balances. Due to these assumptions, the simulation of the FeS_2 electrode requires only the molar volume data for the FeS_2, $Li_3Fe_2S_4$ (Z-phase), Li_2FeS_2 (X-phase), Li_2S, and Fe phases.

The initial porosity of an FeS_2 electrode must be larger than that for the FeS electrode material because the FeS_2 electrode experiences a much larger volume increase upon full discharge than the FeS electrode. Researchers at General Motors build experimental FeS_2 cells with theoretical porosities of 0.30 to 0.50 when fully discharged (to Li_2S and Fe).[21,22] The data given in Table 5 for $\widetilde{V}_{FeS_2}$ and $\widetilde{V}_{Li_2S}$ and $\widetilde{V}_{Fe} = 7.1056$ cm^3/mole can be used to calculate ϵ_+^o from the theoretical ϵ_+^{final}. For example, the theoretical final porosities of 0.30 and 0.50 correspond to initial porosities of 0.727 and 0.805, respectively. For our base-case operating conditions, we use an initial porosity of 0.755.

The relevant Li(Si) electrode data are given in Table 6. The stoichiometric coefficients of the phases in the FeS_2 electrode that are needed for material balances are also given in this table. The molar volume data of pure Li and Si are for 20°C and obtained from Reference 23. The

Table 6. Electrode Data

Li(Si) Electrode		FeS_2 Electrode	
Quantity	Value	Quantity	Value
$x_{Li}^{Li_{3.25}Si}$	0.7647	n_l	2.0
$x_{Si}^{Li_{3.25}Si}$	0.2352	$s_{Li^+,l}$	-2.0
$x_{Li}^{Li_{2.33}Si}$	0.6997	$s_{K^+,l}, s_{Cl^-,l}$	0.0
$x_{Si}^{Li_{2.33}Si}$	0.3003	$s_{FeS_2,a}$	-4/3
$\widetilde{V}_{Li}$	13.093 cm^3/mol	$s_{Z,a}$	2/3
$\widetilde{V}_{Si}$	12.054 cm^3/mol	$s_{Z,b(c)}$	-2
$D_{Li_{3.25}Si}$	7.9×10^{-5} cm^2/s	$s_{X,b(c)}$	4
$D_{Li_{2.33}Si}$	4.9×10^{-5} cm^2/s	$s_{X,d}$	-1
i_o	2.8×10^{-3} A/cm^3	$s_{Li_2S,d}$	2
L_-	0.64 cm	$s_{Fe,d}$	1

diffusion coefficients were obtained from Reference 9. We estimate the molar volumes of the lithium saturated $Li_{3.25}Si$ and $Li_{2.33}Si$ phases from

$$\rho_{Li_{3.25}Si} = \frac{\left(x_{Li}^{Li_{3.25}Si} M_{Li} + x_{Si}^{Li_{3.25}Si} M_{Si} \right)}{\left(x_{Li}^{Li_{3.25}Si} \widetilde{V}_{Li} + x_{Si}^{Li_{3.25}Si} \widetilde{V}_{Si} \right)} \tag{10}$$

and

$$\rho_{Li_{2.33}Si} = \frac{\left(x_{Li}^{Li_{2.33}Si} M_{Li} + x_{Si}^{Li_{2.33}Si} M_{Si} \right)}{\left(x_{Li}^{Li_{2.33}Si} \widetilde{V}_{Li} + x_{Si}^{Li_{2.33}Si} \widetilde{V}_{Si} \right)} , \tag{11}$$

respectively. For the base-case condition of isothermal discharge at 743.15 K with the Li(Si)

negative electrode, U_b is 1.8261 V.

Results and Discussion

Behavior at 470°C and Eutectic Electrolyte Composition.—The solid line in Figure 6 represents the reversible cell voltage for a LiAl/FeS_2 cell discharged at constant temperature. The utilization is defined as

$$\%\text{Utilization of } FeS_2 = \frac{100\ i\ t\ \widetilde{V}_{FeS_2}}{L_+\ \epsilon^s_{FeS_2}\ 4\ F} \tag{12}$$

and may be thought of as a dimensionless time during discharge.

The dashed line in Figure 6 gives the model result for the voltage of the FeS_2 electrode in a LiAl/FeS_2 cell, relative to a LiAl ($\alpha-\beta$) reference electrode placed at the positive electrode-reservoir interface. Four regions of discharge of the FeS_2 electrode can be distinguished. The rounding of the discharge curve, relative to the solid curve is due to irreversibilities associated with ohmic losses, migration effects, mass-transfer, and reaction overpotentials.

At 92% utilization, we predict the 1 V cell cutoff voltage to be reached. This corresponds to approximately 6 hours of discharge. The cell voltage drops at this point because KCl precipitate clogs the pores of the FeS_2 electrode. All the FeS_2 discharge reactions consume lithium ions, which causes the KCl concentration in the positive electrode to increase. If the KCl concentration increases above its saturation value, solid KCl precipitates within the electrode. The onset of KCl precipitation is predicted at 30% utilization; however, by 41.6% utilization the precipitate is not present because it dissolves during the period that reaction c alone occurs within the electrode, and the reaction distribution is nearly uniform. KCl precipitation is initiated a second time, on the final plateau, at 68.6% utilization. KCl precipitation has limited the electrode utilization to 92% utilization. At this point, the cell cutoff voltage is reached.

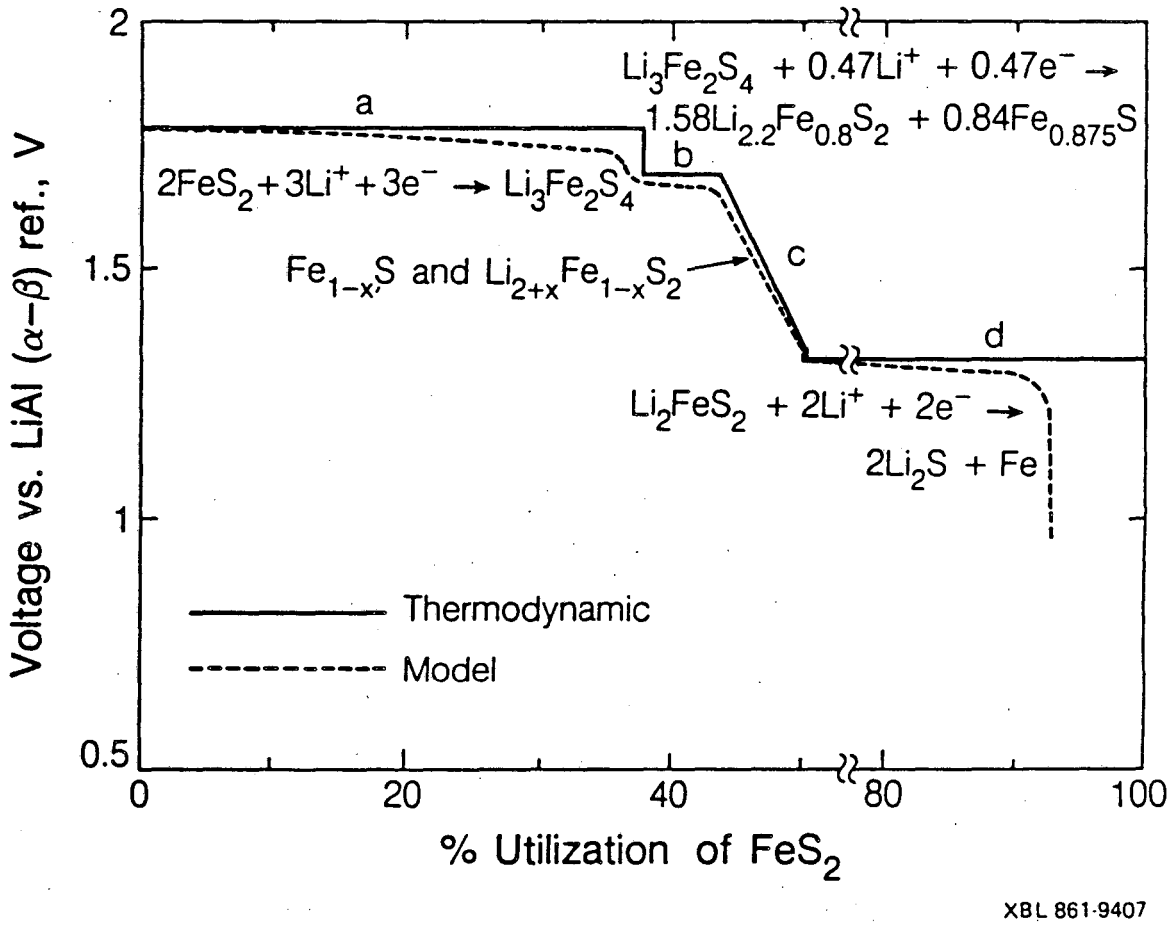

Figure 6. Calculated voltage of the FeS_2 electrode in a $LiAl/FeS_2$ cell relative to a LiAl (α-β) reference electrode placed at the electrode-reservoir interface. The solid curve is for a cell discharged reversibly at 470°C, and the dashed curve is the model result for a discharge current density of 41.6 mA/cm^2 and 58% LiCl electrolyte (base-case operating conditions).

On the first plateau, reaction a is occurring, and the voltage drops at the end of the plateau. The onset of reactions b and c is marked by the voltage leveling, and the FeS_2 is exhausted at 39% utilization. Between these two points, three reactions occur simultaneously within the positive electrode. Reactions b and c occur together at the same position within the electrode, and reaction a occurs in a region located more toward the back of the electrode. Reaction c begins simultaneously with reaction b in irreversible discharge, although it does not proceed rapidly until reaction b is completed at approximately 43.2% utilization.

The solid line in Figure 7 gives the FeS_2-electrode behavior when the discharge current density is increased to 100 mA/cm^2. The onset of the reactions b and c is initiated sooner (21.4% utilization) than for the case with the lower current density because of the increased overpotentials induced by the higher discharge current. The onset of KCl precipitation is predicted to occur at 17.6% utilization. In this case the FeS_2 is not exhausted before the cell cutoff voltage of 1.10 V is reached. The larger discharge current density means that at a given utilization a shorter time period has elapsed. For example, the end of discharge for the 100 mA/cm^2 case (27.8% utilization) is reached after 0.65 hours. For the case with 41.6 mA/cm^2, 27.8% utilization is reached after 1.57 hours of discharge.

The transfer-current density is equal to the divergence of the current density in the pores of the electrode.[3,4] It is also proportional to the reaction rate per unit volume of the electrode. Figure 8 gives the distribution of the total transfer current at the onset of the b and c reactions. The behavior of the transfer-current distribution is understood most easily be examining the potential distribution. The potential distribution is governed by a modified Ohm's law equation.[3,4] We can nondimensionalize this equation and define the different contributions to the potential gradient

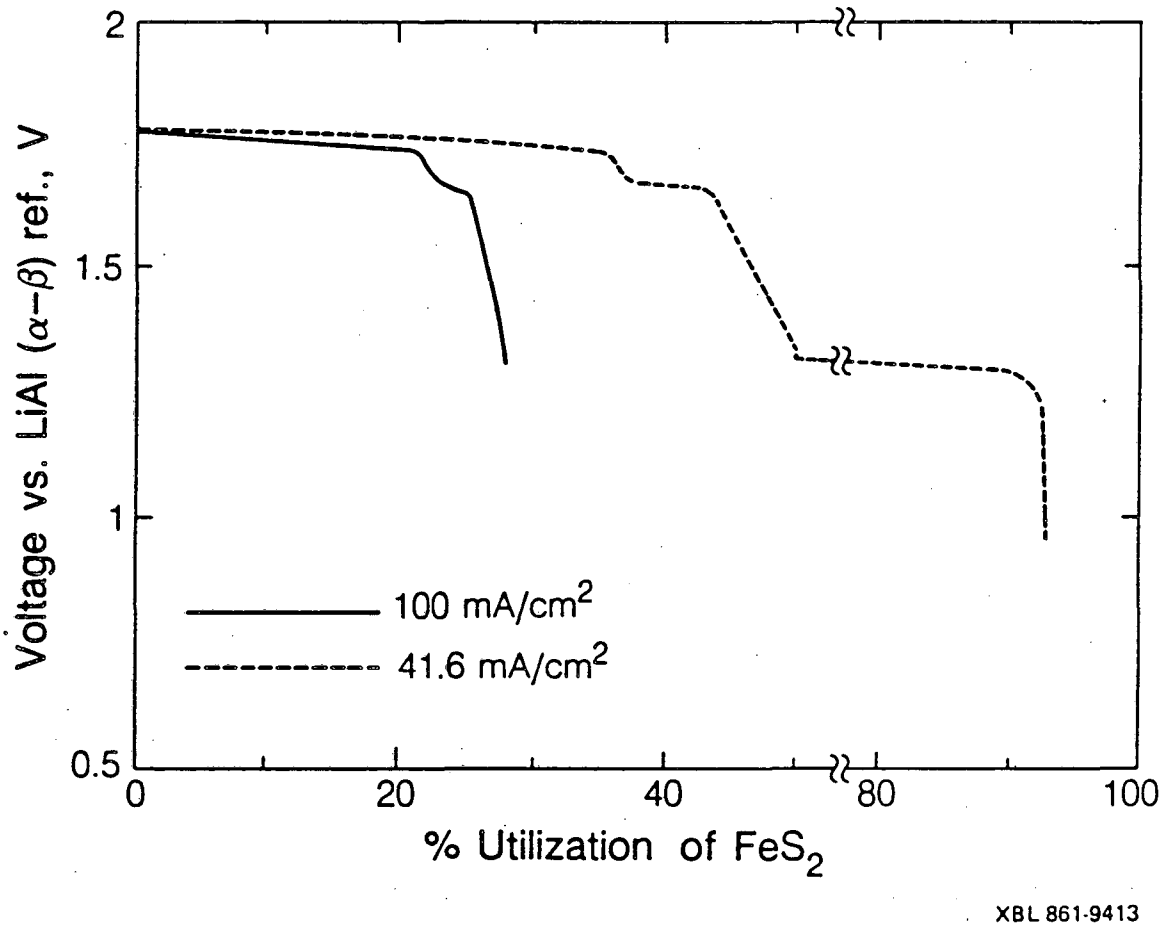

Figure 7. Model results for the voltage of the FeS_2 electrode in a $LiAl/FeS_2$ cell, relative to a LiAl (α-β) reference electrode placed at the electrode-reservoir interface, for two discharge current densities (base-case operating conditions, except for i).

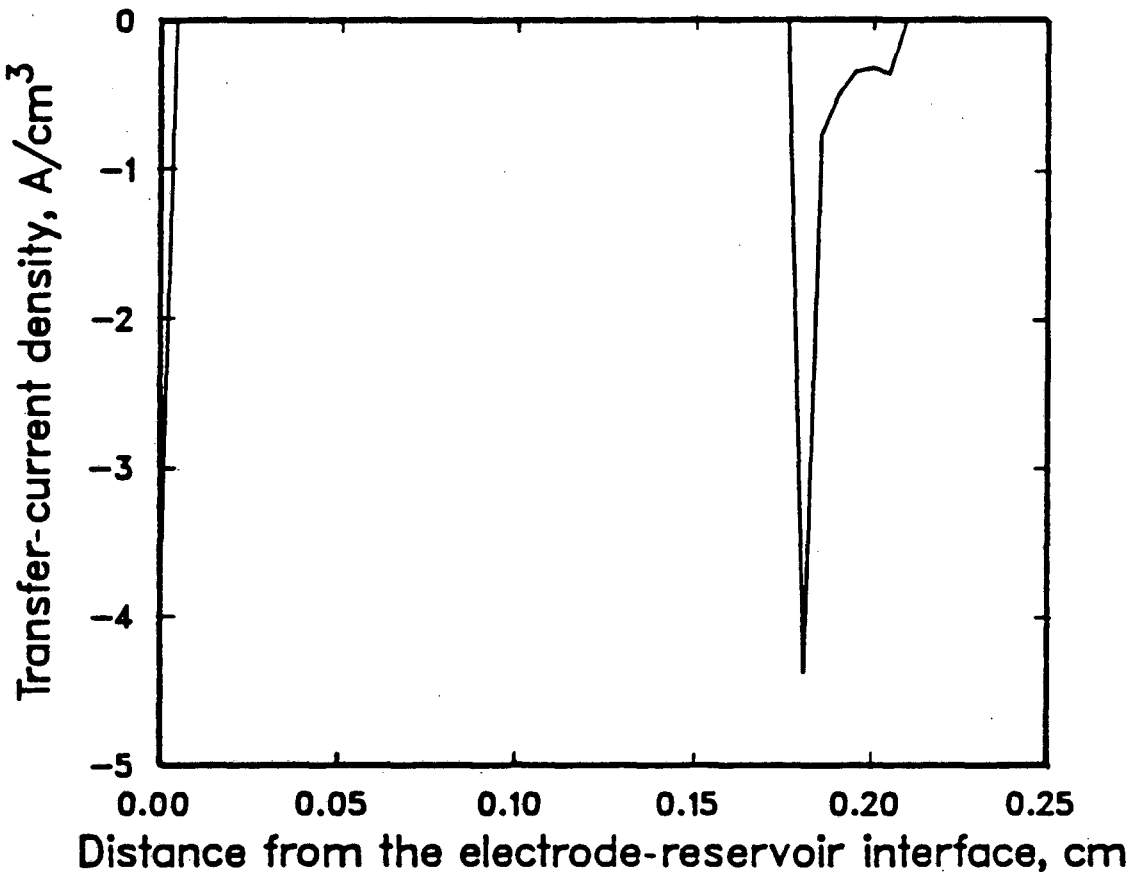

Figure 8. Transfer-current distribution within the FeS_2 electrode at the onset of reactions b and c (parameters as in Figure 7 for the 41.6 mA/cm^2 discharge).

$$\frac{\nabla\eta}{i\left(\frac{1}{\kappa}+\frac{1}{\sigma}\right)} = \frac{\mathbf{i}_{pore}}{i}\frac{\frac{1}{\kappa}}{\left(\frac{1}{\kappa}+\frac{1}{\sigma}\right)} - \frac{\mathbf{i}_{matrix}}{i}\frac{\frac{1}{\sigma}}{\left(\frac{1}{\kappa}+\frac{1}{\sigma}\right)} - \frac{RT}{Fx_{\mathrm{LiCl}}}\frac{\left(1+\frac{d\ \ln\gamma_{\mathrm{LiCl}}}{d\ \ln x_{\mathrm{LiCl}}}\right)\nabla x_{\mathrm{LiCl}}}{i\left(\frac{1}{\kappa}+\frac{1}{\sigma}\right)} \quad (13)$$

$$total = solution\ term + matrix\ term + concentration\ term$$

The quantity i is the sum of the pore and matrix currents. The solution term is proportional to the fraction of current flowing in the electrolyte and the electrolyte's fraction of the total electrode resistance at a given position within the electrode. Analogously, the matrix term is proportional to the fraction of current flowing in the matrix phase and the matrix's fraction of the total electrode resistance at a given point. In the absence of electrolyte concentration variations, these two terms determine the potential distribution. The concentration term accounts for concentration variations and is proportional to $\nabla(\ \ln x_{\mathrm{LiCl}}\ )$.

As shown in Figure 8, the solution current is transferred to the matrix phase at two main positions. These two spikes mark the positions of two reaction fronts. The position of the reaction front for reaction a is deep within the electrode, and electrode reactions do not occur in the region of the electrode between these two fronts. There is a minimum in j_a that is explained by the terms in the Ohm's law equation shown in Figure 9. The minimum in j_a is associated with the total potential gradient passing through zero. The behavior of the potential gradient appears to be dominated by the concentration term. KCl precipitate is present in the reaction zone of reaction a. The electrolyte concentration is constant in this region and is partially responsible for the zero in the gradient of the potential. The solution term also decreases after the position of the reaction front because the fraction of current density in the pore phase is decreasing as current is transferred to the matrix phase.

The reaction front for reactions b and c is at the front of the electrode. Most of the 41.6 mA/cm^2 of current density is transferred to the matrix phase by reaction a (i_a = 31.8 mA/cm^2). The remaining 9.8 mA/cm^2 of current density is transferred to the matrix phase by reactions b

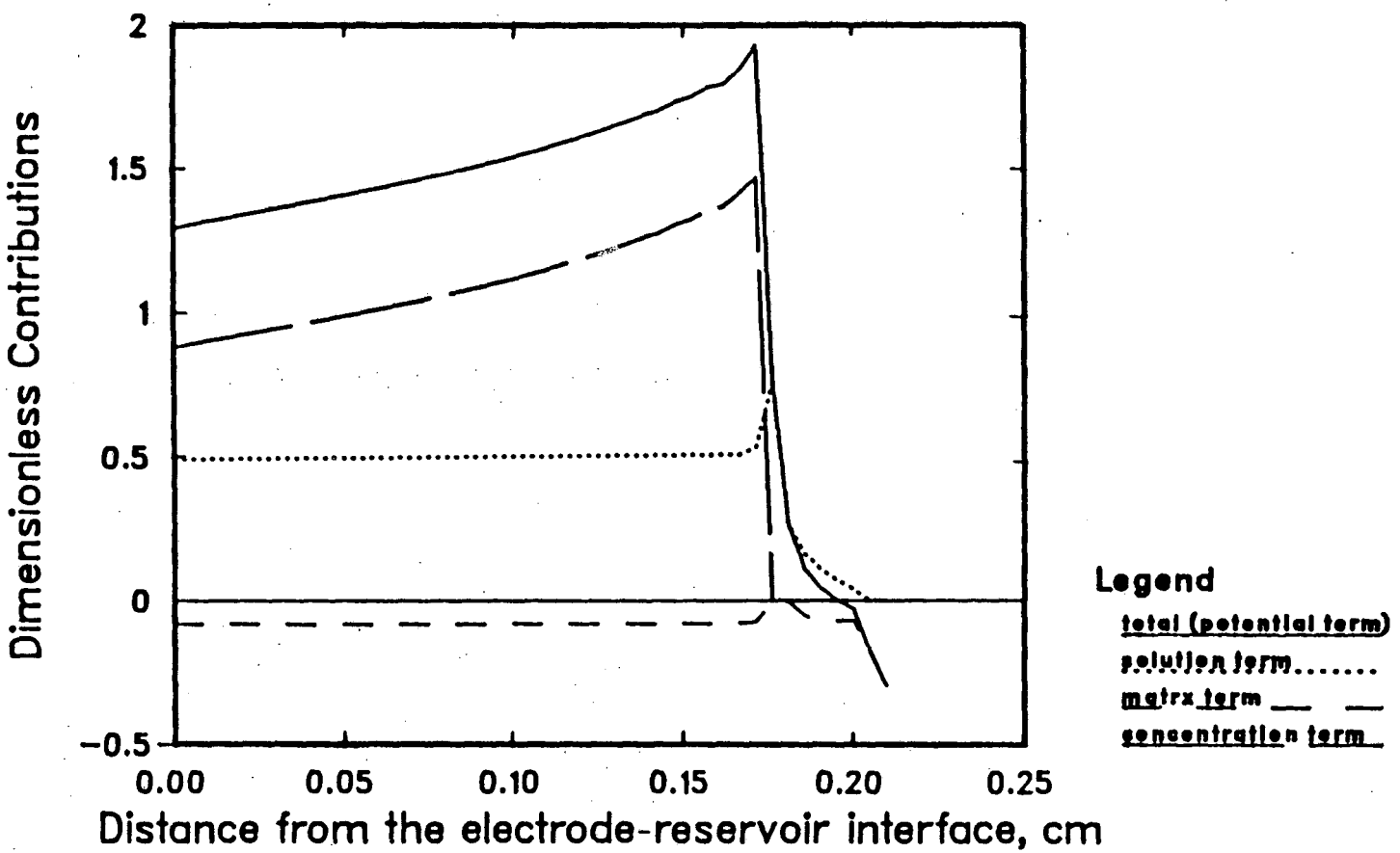

Figure 9. Contributions of terms in the Ohm's law equation (Equation 13) throughout the FeS_2 electrode (corresponding to the case depicted in Figure 8).

and c at the positive electrode-reservoir interface. At the onset of reactions b and c, the surface overpotentials $\eta_{s,b}$ and $\eta_{s,c}$ are negative only at the front of the FeS_2 electrode. At the front of the electrode $j_b = 3.975$ A/cm^3 and $j_c = 0.131$ A/cm^3. The transfer current for reaction c is smaller than reaction b due to the state-of-discharge dependent overpotential.

At 40% utilization, the FeS_2 is exhausted, and eventually the capacity in region b is also exhausted. After this point, reaction c is the only reaction occurring within the electrode.

As discharge proceeds, the reaction distribution becomes more uniform, and at 49.77% utilization the transfer-current distribution is uniform throughout the electrode with a value of 0.195 A/cm^3. The dependency of the surface overpotential on the state-of-discharge forces the reaction zone to penetrate deep into the electrode, unlike the behavior of the reaction zone depicted in Figure 8. After 49.77% utilization, the capacity in region c becomes exhausted at the front of the electrode, and the exhausted area moves deeper into the electrode as discharge proceeds.

At 49.99% utilization, the surface overpotential $\eta_{s,d}$ at the front of the electrode becomes negative, this marks the onset of reaction d. The behavior of the reaction zone for reaction d is similar to that of reaction a. It is a sharp zone that starts at the front of the electrode and moves through the electrode as X-phase is converted to Li_2S and Fe.

Figure 10 gives the model results for the voltages of electrodes relative to a two-phase LiAl ($\alpha-\beta$) reference electrode placed at the positive electrode-reservoir interface. The upper, dashed line gives the potential of the FeS_2 electrode in a LiAl/FeS_2 cell, relative to this reference electrode. The lower dashed line gives the potential of the LiAl negative electrode relative to this reference electrode; the difference between the two dashed curves, is the cell voltage.

The results of the Li(Si)/FeS_2 cell discharged only on the upper-upper plateau of the positive electrode are shown by the solid curves. The behavior of the FeS_2 electrode appears to be

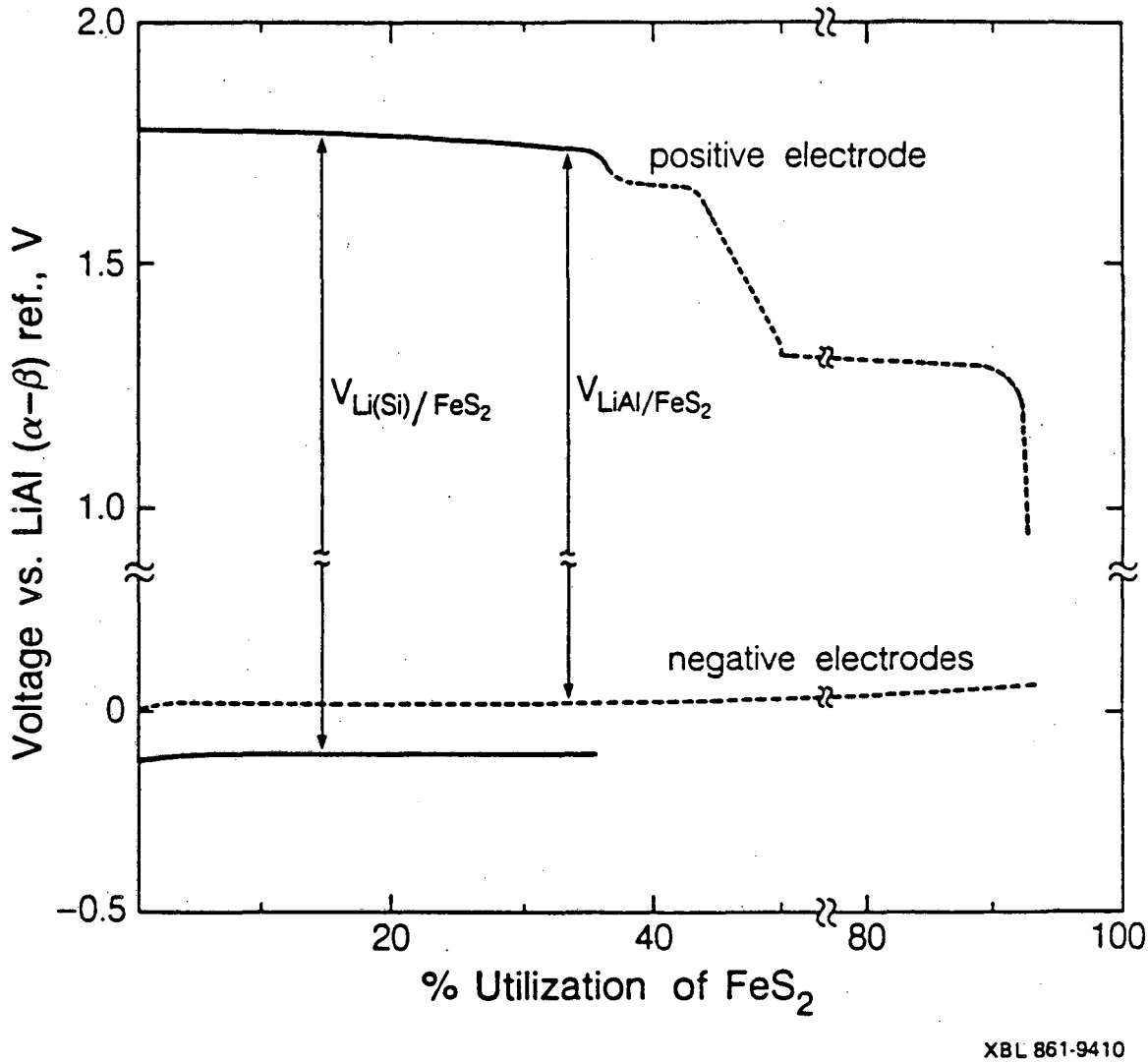

Figure 10. Model results for the potential of electrodes in a Li(alloy)/FeS_2 cell relative to a LiAl (α-β) reference electrode placed at the positive electrode-reservoir interface (base-case operating conditions).

independent of the negative electrode. We presume that the potential of the positive electrode in the Li(Si)/FeS_2 cell would yield approximately the same potential as in the LiAl/FeS_2 cell if we chose to discharge to greater depths. As shown by this figure, a larger cell voltage is obtained for the cell with the Li(Si) electrode, relative to the cell with LiAl as a negative electrode.

Behavior at 450°C and Lithium-Rich Electrolyte.—One of the most important aspects of modeling is to compare model results with experimental results. The more agreement that is seen, the more confident we are with our understanding of how a system works. Figure 11 compares model and experimental results[21] for the FeS_2 electrode behavior in a LiAl/FeS_2 cell at 450°C, 50 mA/cm^2, and 68% LiCl electrolyte. The reversible discharge behavior is also shown in this figure. The 4 regions of discharge of the FeS_2 electrode can be distinguished in the experimental curve. As we discussed earlier, there is some controversy in the literature[6,7] concerning different regions of discharge for the FeS_2 electrode. The results of Figure 11 give some credence to the "4-region" behavior of the FeS_2 electrode.

The spike at the beginning of discharge is a common observation in experimental FeS_2 cells, and we do not predict it with our mathematical model. We can postulate three possible reasons for the initial voltage spike. One explanation is the presence of a highly reactive impurity. Secondly, the spike may be due to the reaction of liquid sulfur formed by over-charging the electrode. Another possibility is that the Li-Fe-S phase diagram may not be complete. For example, FeS_2 may exhibit some degree of nonstoichiometry, and the point on the diagram may actually be part of a single-phase segment. This region would not have much lithium capacity and would give rise to a sharp voltage drop on discharge.

We can also contrast the start of region d in the model and experimental results. Region d begins at less than 50% utilization in the experimental cell, which indicates that some of the capacity of the electrode has been lost. We do not predict this capacity loss with our

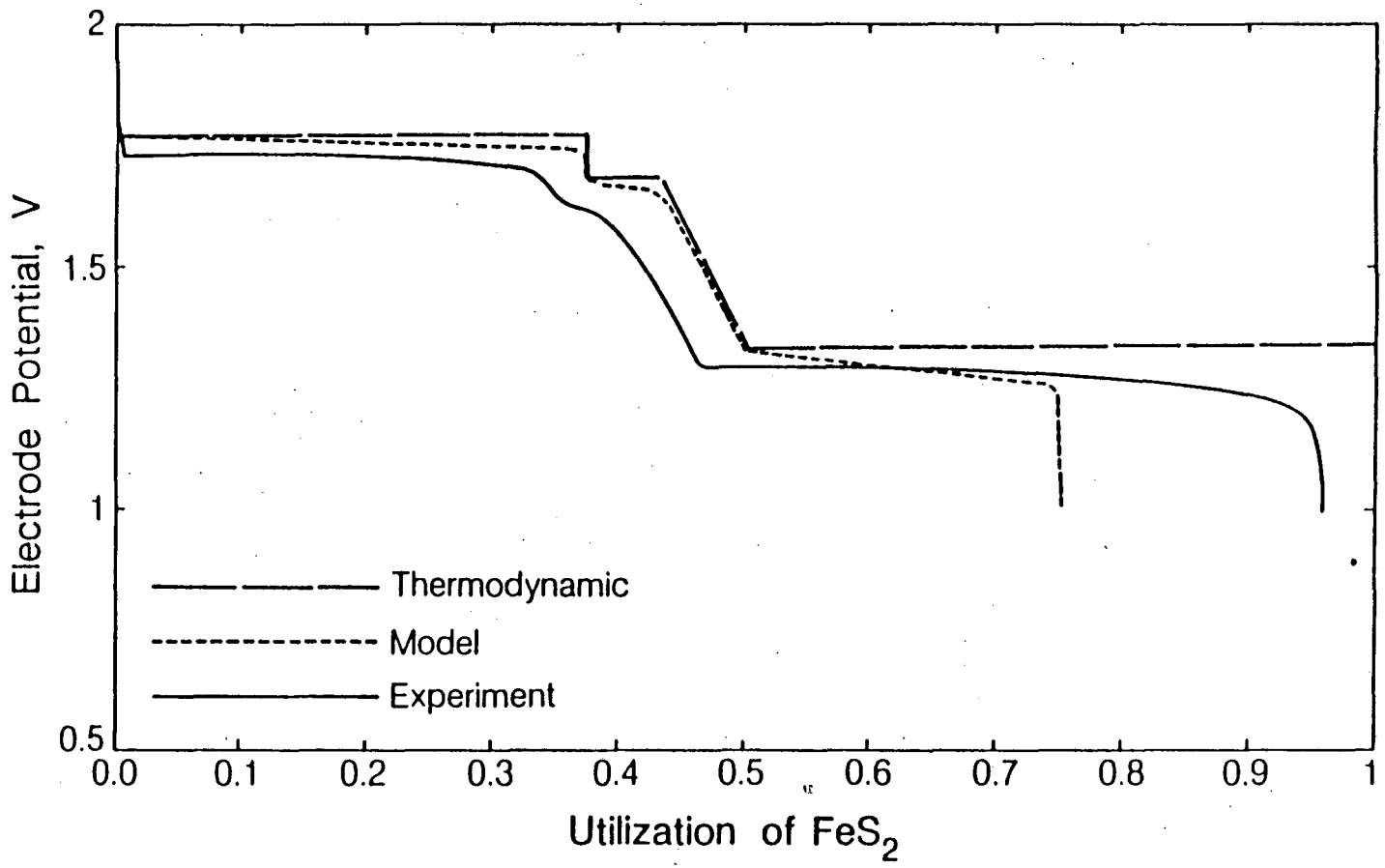

XBL 861-9402

Figure 11. Comparison of model and experimental results[21] for the voltage of the FeS_2 electrode in a $LiAl/FeS_2$ cell, relative to a LiAl (α-β) reference electrode (450°C, 50 mA/cm^2, 68% LiCl electrolyte). The model has the reference electrode placed at the electrode-reservoir interface, and the experiment has the reference electrode placed within the separator. The reversible, thermodynamic potential is also shown in order to display more clearly the losses of the system.

mathematical model. The capacity loss problem with experimental cells has been studied by several researchers. The weight loss of FeS_2 due to evolution of sulfur vapor in an argon atmosphere has been determined as a function of temperature.[24] The FeS_2 samples demonstrated stability at 300°C and severe weight loss at 450°C. The capacity loss of the electrode is also, however, dependent upon the electrolyte and potential. Weppner *et al.*[7] were able to obtain a stable voltage reading in the $S-FeS_2-Li_2S$ region (see Figure 1) with molten, eutectic, LiCl-KCl electrolyte at 400°C, but not with solid-state $Li_4SiO_4 - Li_3PO_4$ electrolyte. Stable voltage readings were obtained for all other measurements with the solid-state electrolyte. Figure 12 demonstrates the capacity loss after 80 charge-discharge cycles observed by Dunning *et al.*[21] for a temperature of 450°C and lithium-rich electrolyte (68% LiCl). It was also observed that the rate of capacity loss is higher in the lithium rich than the eutectic electrolyte.

The voltage drop shown for the experimental cell in Figure 11 is probably due to the exhaustion of X-phase, since greater than 50% of the electrode's capacity in region d is not possible (region d spans from 45-95% utilization). The voltage drop to the cutoff point in the model result is due to the clogging of the pores with KCl precipitate. Under certain operating conditions, a loss of capacity in region d is observed experimentally[22] and may be explained by KCl precipitation. If the capacity loss in region d is caused by KCl precipitation, utilization in region d should increase with temperature, x^o_{LiCl}, and ϵ^o_+. All of these trends are observed experimentally.[22] It is appropriate here to recall that in Figure 7 (for the case of 100 mA/cm^2) the model predicted that KCl precipitation contributed to the apparent shortening of the upper plateau. The effects of KCl precipitation on the performance of model the FeS electrodes are discussed in References 12 and 13.

At 13% utilization of FeS_2, LiCl precipitation is observed in the LiAl negative electrode; the precipitation of LiCl, however, does not limit the utilization of the electrode's active material.

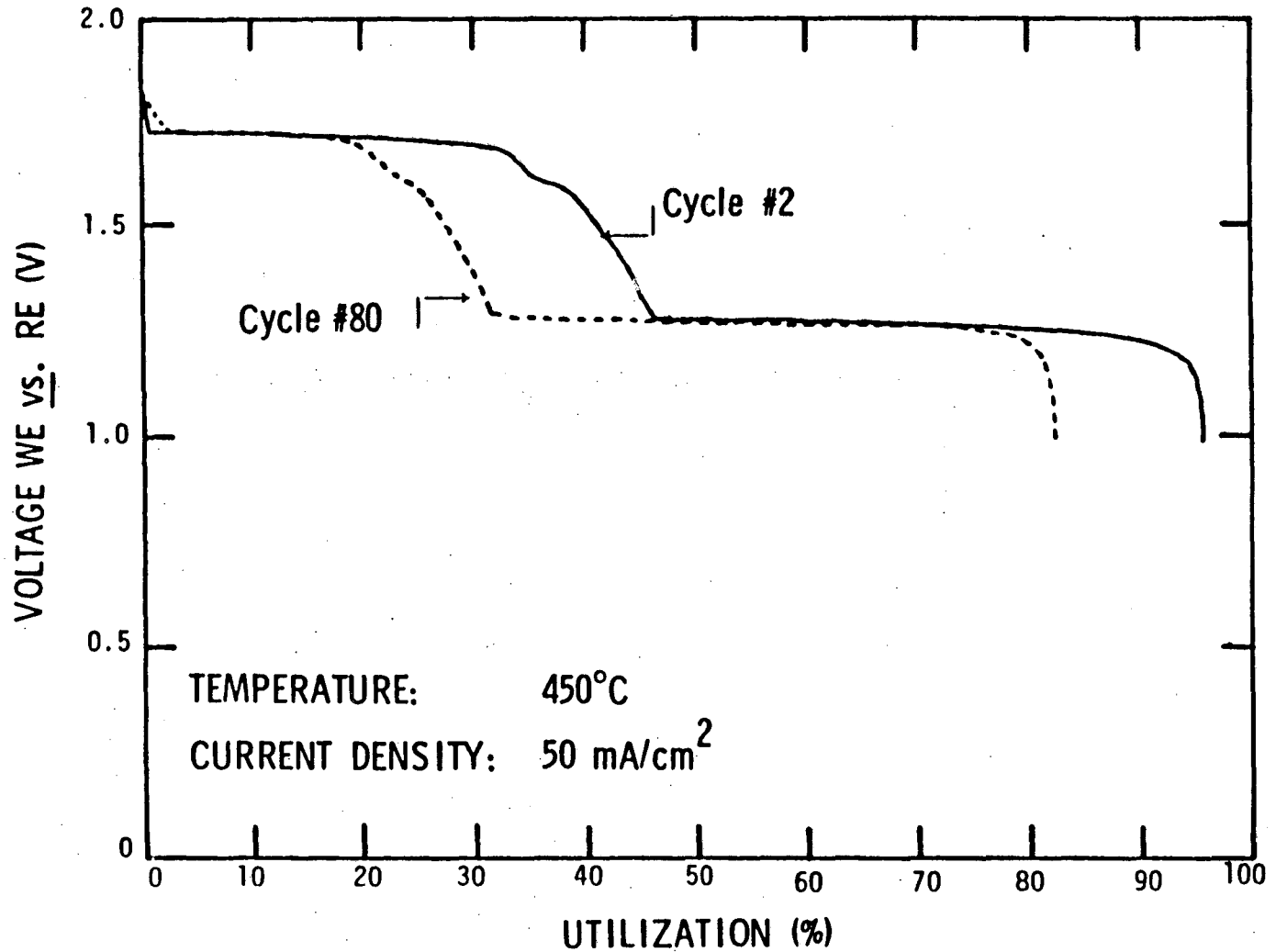

Figure 12. Experimental FeS_2 electrode potential after 2 cycles (also shown in Figure 11) and after 80 cycles in a $LiAl/FeS_2$ cell, relative to a reference electrode placed in the separator[21] (conditions are 450°C and 50 mA/cm^2).

Some of the more recent work directed toward the capacity loss problem in experimental cells should be mentioned. As we discuss above, the capacity loss of the FeS_2 electrode should decrease with decreasing temperature. Kaun[25] proposes an electrolyte with a lower melting point (310°C) and broader liquidus than LiCl-KCl electrolyte. His electrolyte, $x_{LiCl} = 0.25$, $x_{LiBr} = 0.38$, $x_{KBr} = 0.37$, allows lower cell operating temperatures of 390 to 400°C. Kaun operates $LiAl/FeS_2$ cells only on the upper plateau of the FeS_2 electrode (regions a, b, and c) where X-phase is the final discharge product. There is a much smaller volume change on discharge of this cell than in a cell that is discharged to Li_2S and Fe; hence Kaun uses cells with dense positive electrodes ($\epsilon_+^o = 0.5$). The cell capacity remains constant through more than 300 cycles at 50 mA/cm^2 and a temperature of 397°C. This is a substantial improvement over the more conventional $LiAl/FeS_2$ cells (discharged to Li_2S and Fe) built in their laboratory. These conventional cells operate at 427°C with LiCl-KCl electrolyte and lose 30% of their capacity after 200 cycles (also see Figure 12).

There are other disadvantages to high operating temperatures than capacity loss of the FeS_2 electrode; for example, there are increases in corrosion of cell components at higher operating temperatures. Operating these cells at lower temperature may lessen the high-temperature problems. Also, operation only on the upper plateau of the FeS_2 electrode has the advantage of a relatively constant voltage throughout the cell discharge. This is important because there may be applications for these cells that could not tolerate large voltage change between the upper-upper plateau (region a) and the lower plateau (region d), which occurs between 37.5 and 50% utilization. It would be interesting, however, to investigate experimentally a $LiAl/FeS_2$ cell discharged through the lower plateau with Kaun's electrolyte and the low operating temperature of 397°C.

Conclusions

The equilibrium voltage behavior of a Li(Si)/FeS_2 cell exhibits many regions (up to six) and can vary as much as 0.6 V during discharge. This must be considered in the design of these cells because there may be applications that will not tolerate the large voltage changes during discharge.

All of the regions in the discharge of a Li(Si)/FeS_2 cell are endothermic except the region in which reaction d of the FeS_2 electrode occurs. Therefore, to maintain isothermal operation, a Li(Si)/FeS_2 cell discharged reversibly would require external heating, up to 50% utilization of FeS_2, and cooling after 50% utilization.

The agreement between the model and experimental results supports the "4-region" behavior of the FeS_2 electrode. The experimentally observed capacity loss problem on the upper voltage plateau during discharge must be solved if the system is to be practical. Our model predicts that KCl precipitation can limit the utilization of the FeS_2 electrode, usually on the lower voltage plateau. The capacity loss due to KCl precipitation should decrease with increasing temperature, LiCl concentration in the electrolyte, and porosity of the electrode. For certain operating conditions, limitations on the utilization of the lower voltage plateau are observed experimentally and are probably due to KCl precipitation.

Acknowledgment

This work was supported by the Assistant Secretary of Conservation and Renewable Energy, Office of Energy Systems Research, Energy Storage Division of the United States Department of Energy under Contract Number DE-AC03-76SF00098.

List of Symbols

a	interfacial area per unit electrode volume, cm^{-1}
a_l	constant in the expression for the open-circuit potential of reaction l, V
b_l	temperature coefficient in the expression for the open-circuit potential of reaction l, V/K
D	diffusion coefficient, cm^2/sec
e^-	symbol for an electron
F	Faraday's constant, 96,487 C/equiv
i	current density, A/cm^2
$i_{o,l}$	exchange current density for electrode reaction l, A/cm^2
j	transfer current density per unit volume of electrode, A/cm^3
L	length of cell, cm
m	precipitation parameter
M_i	molecular weight of species i
q_l	capacity for reaction l (see Equation 7), C/cm^3
R	universal gas constant, 8.3143 J/mol-K
$s_{i,l}$	stoichiometric coefficient of species i in reaction l
t	time, s
T	absolute temperature, K

U_l theoretical open-circuit potential for reaction l, relative to a reference electrode, V

$U_{l,o}$ theoretical open-circuit potential for reaction l at the local composition within the electrode, relative to a reference electrode that is taken to be the same kind as the second reaction in the discharge mechanism, V

$\widetilde{V}$ molar volume, $cm^3/mole$

x, x' composition variables in nonstoichiometric compounds

x_i mole fraction of species i

y composition variable in a nonstoichiometric compound

Greek letters

α_a transfer coefficient in the anodic direction

α_c transfer coefficient in the cathodic direction

β the mole ratio of $Li_{3.25}Si$ to FeS_2

ϵ porosity or electrolyte volume fraction

ϵ_i volume fraction of species i

$\gamma_{i,j}$ activity coefficient of species i in phase j

η overpotential, defined as the difference of the matrix and pore-solution potentials, V

$\eta_{s,l}$ surface overpotential of reaction l, V

κ effective ionic electrolyte conductivity, $(\Omega\text{-cm})^{-1}$

ρ density, g/cm^3

σ solid-phase electrical conductivity, $(\Omega\text{-cm})^{-1}$

Subscripts

ccp current collector in the positive electrode

eff effective

i refers to a species

l refers to a reaction

matrix refers to the solid electrode matrix

pore refers to the pores of an electrode

+ positive electrode

− negative electrode

Superscripts

final at end of discharge

o refers to secondary reference state or initial

References

1. E. C. Gay, R. K. Steunenberg, W. E. Miller, J. E. Battles, T. D. Kaun, F. J. Martino, J. A. Smaga, and A. A. Chilenskas, in *Li-Alloy/FeS Cell Design and Analysis Report,* Argonne National Laboratory Report ANL-84-93 (July, 1985).

2. J. R. Selman, "Molten-Salt Battery Cells with Sulfur or Metal Sulfide Electrodes," R. P. Tischer, ed., *The Sulfur Electrode,* Academic Press, New York, New York, pp. 219-232 (1983).

3. R. Pollard, *Mathematical Modeling of the Lithium-Aluminum, Iron Sulfide Battery,* Dissertation, University of California, Berkeley (1979).

4. R. Pollard and J. Newman, "Mathematical Modeling of the Lithium-Aluminum, Iron Sulfide Battery. I. Galvanostatic Discharge Behavior," *Journal of the Electrochemical Society,* **128**, 491-502 (March, 1981).

5. R. Pollard and J. Newman, "Mathematical Modeling of the Lithium-Aluminum, Iron Sulfide Battery. II. The Influence of Relaxation Time on the Charging Characteristics," *Journal of the Electrochemical Society,* **128**, 503-507 (March, 1981).

6. Z. Tomczuk, B. Tani, N. C. Otto, M. F. Roche, and D. R. Vissers, "Phase Relationships in Positive Electrodes of High Temperature Li-Al/LiCl-KCl/FeS_2 Cells," *Journal of the Electrochemical Society,* **129**, 925-931 (May, 1982).

7. J. A. Schmidt and W. Weppner, "Phase Equilibria and Thermodynamics of Li - Fe - S," E. F. Bertaut *et al.*, eds., *Proc. 7th Int. Conf. on Solid Compounds of Transition Elements*, Grenoble, France: I B 13 (1982).

8. J. A. Schmidt and W. Weppner, "Kinetics of Compositional Variations in the Ternary Sys-

tem Li - Fe - S," The Electrochemical Society *Extended Abstracts* for the Montreal, Canada, Meeting, Volume 82-1, Abstract 344, page 562 (May, 1982).

9. C. J. Wen and R. A. Huggins, "Chemical Diffusion in Intermediate Phases in the Lithium-Silicon System," *Journal of Solid State Chemistry,* **37**, 271-278 (1981).

10. Z. Tomczuk, S. K. Preto, and M. F. Roche, "Reactions of FeS Electrodes in LiCl-KCl Electrolyte," *Journal of the Electrochemical Society,* **128**, 760-772 (April, 1981).

11. Z. Tomczuk, M. F. Roche, and D. R. Vissers, "Emf Measurements on the Li-Al/FeS Couple in LiF-LiCl-LiBr Electrolyte," *Journal of the Electrochemical Society,* **128**, 2255-2256 (October, 1981).

12. D. M. Bernardi, *Mathematical Modeling of Lithium(alloy), Iron Sulfide Cells and the Electrochemical Precipitation of Nickel Hydroxide,* Dissertation, University of California, Berkeley (1986).

13. D. Bernardi, E. Pawlikowski, and J. Newman, "Mathematical Modeling of LiAl/LiCl-KCl/FeS Cells," to be submitted to the *Journal of the Electrochemical Society.*

14. Z. Tomczuk and D. R. Vissers, in *Lithium/Iron Sulfide Batteries for Electric-Vehicle Propulsion and other Applications,* Argonne National Laboratory Report ANL-83-62, page 19 (1983).

15. Z. Tomczuk, Argonne National Laboratory, personal communication (1982).

16. H. Rau, "Energetics and Defect Formation and Interaction in Pyrrhotite $Fe_{1-x}S$ and Its Homogeneity Range," *Journal of the Physics and Chemistry of Solids,* **37**, 425-429 (1976).

17. M. Roche, Argonne National Laboratory, personal communication (1982).

18. R. A. Sharma and R. N. Seefurth, "Thermodynamic Properties of the Lithium-Silicon

System," *Journal of the Electrochemical Society,* **123**, 1763-1768 (December, 1976).

19. L. Redey and D. R. Vissers, in *Lithium/Iron Sulfide Batteries for Electric-Vehicle Propulsion and other Applications,* Argonne National Laboratory Report ANL-83-62, page 8 (1983).

20. J. Newman, *Electrochemical Systems,* Prentice-Hall, Englewood Cliffs, New Jersey (1973).

21. J. S. Dunning, in *Lithium/Iron Sulfide Batteries for Electric-Vehicle Propulsion and other Applications,* Argonne National Laboratory Report ANL-80-128, pages 190-198 (February, 1981).

22. J. S. Dunning, in *High Performance Batteries for Electric-Vehicle Propulsion and Stationary Energy Storage,* Argonne National Laboratory Report ANL-79-94, pages 61-67 (March, 1981).

23. R. C. Weast, *Handbook of Chemistry and Physics,* 48th Edition, CRC Press, Cleveland, Ohio (1967).

24. H. F. Gibbard, "Investigation of the Mechanism for Capacity Decline of the FeS_2 Electrode in Lithium/Iron Disulfide Cells," *Technology Base Research Project for Electrochemical Energy Storage. Annual Report for 1984,* Lawrence Berkeley Laboratory, LBL-19545, pp. 36-37 (May, 1985).

25. T. D. Kaun, "Li-Al/FeS_2 Cell with LiCl-LiBr-KBr Electrolyte," *Journal of the Electrochemical Society,* **132**, 3063-3064 (December, 1985).

This report was done with support from the Department of Energy. Any conclusions or opinions expressed in this report represent solely those of the author(s) and not necessarily those of The Regents of the University of California, the Lawrence Berkeley Laboratory or the Department of Energy.

LAWRENCE BERKELEY LABORATORY
TECHNICAL INFORMATION DEPARTMENT
UNIVERSITY OF CALIFORNIA
BERKELEY, CALIFORNIA 94720